Drug diffusivities in nanofibrillar cellulose hydrogel by combined time-resolved Raman and fluorescence spectroscopy

Zini, Jacopo

2021-06-10

Zini , J , Kekkonen , J , Kaikkonen , V A , Laaksonen , T , Keränen , P , Talala , T , Mäkynen , A J , Yliperttula , M & Nissinen , I 2021 , ' Drug diffusivities in nanofibrillar cellulose hydrogel by combined time-resolved Raman and fluorescence spectroscopy ' , Journal of Controlled Release , vol. 334 , pp. 367-375 . https://doi.org/10.1016/j.jconrel.2021.04.032

http://hdl.handle.net/10138/332498
https://doi.org/10.1016/j.jconrel.2021.04.032

Journal of Controlled Release 334 (2021) 367–375

Contents lists available at ScienceDirect

Journal of Controlled Release

journal homepage: www.elsevier.com/locate/jconrel

Drug diffusivities in nanofibrillar cellulose hydrogel by combined time-resolved Raman and fluorescence spectroscopy

Jacopo Zini [a], Jere Kekkonen [b], Ville A. Kaikkonen [c], Timo Laaksonen [a], Pekka Keränen [b], Tuomo Talala [b], Anssi J. Mäkynen [c], Marjo Yliperttula [a,*,1], Ilkka Nissinen [b,1]

[a] Division of Pharmaceutical Biosciences, Drug Research Program, Faculty of Pharmacy, University of Helsinki, 00014 Helsinki, Finland
[b] Circuits and Systems Research Unit, University of Oulu, 90014 Oulu, Finland
[c] Optoelectronics and Measurement Techniques Research Unit, University of Oulu, 90014 Oulu, Finland

ARTICLE INFO

Keywords:
Raman
Fluorescence
Drug diffusion
Label-free
Real-time
Nanofibrillated cellulose hydrogel
Anionic nanofibrillated cellulose hydrogel

ABSTRACT

Hydrogels, natural and synthetic origin, are actively studied for their use for implants and payload carriers. These biomaterials for delivery systems have enormous potential in basic biomedical research, drug development, and long-term delivery of biologics. Nanofibrillated cellulose (NFC) hydrogels, both natural and anionic (ANFC) ones, allow drug loading for immediate and controlled release via the slow drug dissolution of solid drug crystals into hydrogel and its subsequent release. This property makes NFC originated hydrogels an interesting non-toxic and non-human origin material as drug reservoir for long-term controlled release formulation or implant for patient care. A compelling tool for studying NFC hydrogels is Raman spectroscopy, which enables to resolve the chemical structures of different molecules in a high-water content like hydrogels, since Raman spectroscopy is insensitive to water molecules. That offers real time investigation of label-free drugs and their release in high-water-content media. Despite the huge potential of Raman spectroscopy in bio-pharmaceutical applications, the strong fluorescence background of many drug samples masking the faint Raman signal has restricted the widespread use of it. In this study we used a Raman spectrometer capable of suppressing the unpleasant fluorescence background by combining a pulsed laser and time-resolved complementary metal-oxide-semiconductor (CMOS) single-photon avalanche diode (SPAD) line sensor for the label-free investigation of Metronidazole and Vitamin C diffusivities in ANFC. The results show the possibility to modulate the ANFC-based implants and drug delivery systems, when the release rate needs to be set to a desired value. More importantly, the now developed label free real-time method is universal and can be adapted to any hydrogel/drug combination for producing reliable drug diffusion coefficient data in complex and heterogeneous systems, where traditional sampling-based methods are cumbersome to use. The wide temporal range of the time-resolved CMOS SPAD sensors makes it possible to capture also the fluorescence decay of samples, giving rise to a combined time-resolved Raman and fluorescence spectroscopy, which provides additional information on the chemical, functional and structural changes in samples.

1. Introduction

Hydrogels are a promising class of materials both as implantable systems for tissue engineering, and as a basis for controlled drug release and delivery. In hydrogels, a network of inter-connected pores enables an efficient retention of water, and transport of oxygen, nutrients and waste products [1]. These implantable matrices should be biomaterials, which will provide mechanical support when used as implanted payload carriers. An ideal biomaterial for controlled drug delivery should mimic the ultrastructure and mechanical properties of native extra-cellular matrix (ECM) with the maintenance of biochemical and physical signals. In essence, the implanted delivery systems should be compatible in stiffness with the cellular environment that is identical to the native state of the particular cell type or tissue to be treated. Such optimized

* Corresponding author.
E-mail addresses: jacopo.zini@helsinki.fi (J. Zini), jere.kekkonen@oulu.fi (J. Kekkonen), ville.kaikkonen@oulu.fi (V.A. Kaikkonen), timo.laaksonen@helsinki.fi (T. Laaksonen), pekka.keranen@oulu.fi (P. Keränen), tuomo.talala@oulu.fi (T. Talala), anssi.makynen@oulu.fi (A.J. Mäkynen), marjo.yliperttula@helsinki.fi (M. Yliperttula), ilkka.nissinen@oulu.fi (I. Nissinen).
[1] Co-last persons

https://doi.org/10.1016/j.jconrel.2021.04.032
Received 21 February 2021; Received in revised form 23 April 2021; Accepted 25 April 2021
Available online 28 April 2021

biomaterials for delivery systems have enormous potential in basic biomedical research, drug development, and long-term delivery of biologics.

Hydrogels from both synthetic and natural sources have been used for implants, and in addition different kinds of polysaccharides have been used as implants and payload carriers, but typically these require a separate cross-linking step to form a proper hydrogel network [2]. In contrast, the native nanofibrillated cellulose (NFC) produced in bacteria and plants [3] forms hydrogels composed of a network of cellulose nanofibers without additional chemical modifications. They have mechanically strong native crystalline structure, lateral dimensions in the nanometer length scale, and exhibit high aspect ratios [4]. NFC can be isolated from plant cell walls using intensive mechanical shearing combined with chemical and enzymatic pre-treatments, and the anionic NFC (ANFC) can be obtained via TEMPO oxidation [4–6]. In aqueous environment, the NFC and ANFC form hydrogels even at low concentrations, typically down to 0.1–0.2 wt% (Ref M4) enabling the control of loss (G') and storage modulus (G") of the hydrogels and encourages their use as an implantable controlled delivery material. NFC hydrogels allows drug loading for both immediate and controlled release via the slow drug dissolution of solid drug crystals into NFC and its subsequent release [6]. This property makes ANFC hydrogels an interesting non-toxic and non-human origin material as drug reservoir for long-term controlled release formulation or implant for patient care. Although the plant derived native nanofibrillar cellulose has not yet found applications in tissue engineering, its potential for wound healing applications has already been shown [7,8]. Critically, in order to produce and modulate the NFC and ANFC based drug delivery hydrogels, the diffusivities of the payloads, i.e. drug molecules, nanoparticles, or vesicles, has to be known. Here, the label-free measurements for their characterization would be extremely beneficial and needed.

The importance of the transport properties of controlled-release in biological systems has been recently reviewed by A.C.Ribeiro and M.A. Esteso [9], who focused on understanding the physical chemistry of carrier-mediated transport phenomena in controlled drug release systems. They combined Raman spectroscopy with the analysis of pulse voltammetry, nuclear magnetic resonance (NMR), ultrasonic relaxation and dissolution kinetics. In addition, M.P.di Cagno et al. [10] recently used UV absorption detection in unstirred aqueous environment to measure the exact concentrations of the drugs and were successfully able to evaluate the drug diffusion coefficients. UV-based systems, however, lack the possibility to follow the stability of the drugs, since the UV-absorption is virtually always detected only in one wavelength, and even in the best of cases cannot reach the sensitivity of vibrational spectroscopy.

Raman spectroscopy is a widely used method to resolve the chemical structure of different molecules especially in samples having a high-water content since Raman spectroscopy, is insensitive to water molecules [11]. Therefore, it offers the possibility for label-free investigation of drugs and their release in high-water-content media. There are several studies presenting the use of Raman spectroscopy or confocal Raman microscopy for drug product analysis [12]. In these systems, the main aim is to have the spatial resolution of the excipients in drug products and the Raman analysis are performed in solid state. F.G.Vogt and M. Stromeir combined UV Raman microscopy analyses to diffuse reflectance UV – visible and fluorescence spectroscopy with conventional bulk Raman spectroscopy [13]. Although all the studies were performed in solid state, their study highlights the need for the combination analysis of several spectroscopic methods. That was already suggested by S. Wartenwig and R.H.H. Neubert in 2005 at their review for the pharmaceutical applications of Raman spectroscopy [14]. They suggested that the mid-IR and Raman spectroscopy are versatile tools in the field of bio- and pharmaceutics, with a wide field of applications ranging from characterization of drug formulations to elucidation of kinetic processes in drug delivery. Another example of the use of Raman spectroscopy in biomedical applications is the use of Raman imaging to detect the amount of hyaluronic acid increase of extracellular matrix deposition in human dermal fibroblasts [15]. The Raman imaging results indicated the macromolecule- and cell type- dependent effects on matrix assembly, turnover, and stiffness in cell-derived matrices.

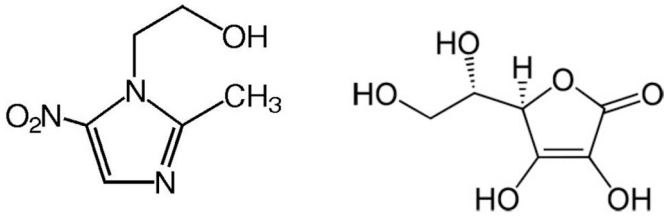

Fig. 1. Chemical structure of Metronidazole, MW 171.15 g/mol (left) and Vitamin C i.e. Ascorbic Acid, MW 176.12 g/mol (right).

Despite the huge potential of Raman spectroscopy in biomedical and pharmaceutical applications, there is a major issue that has restricted the widespread use of this powerful optical tool. The problem has been the strong fluorescence of many samples, including most drugs, that can mask the faint Raman signal [16]. An effective method to suppress the unpleasant fluorescence background is to use short pulsed lasers (~100 ps) and time-gated detectors [17]. The time constant of fluorescence emission, which is typically in the scale of nanoseconds, is relatively long compared to the instantaneous process of Raman scattering. Therefore, by enabling the detector to collect photons only during the laser pulses, all the Raman scattered photons can be collected while simultaneously rejecting most of the fluorescence and other background photons from ambient light. Even though time-gating provides effective fluorescence and background suppression, the restricting challenge with time-gated devices has been their high complexity and costs. Traditionally, time-gated detectors have been implemented by means of techniques such as ultrafast time-gated intensified charge-coupled device cameras and optical Kerr gates coupled with detectors, which are sophisticated and bulky laboratory-only solutions [18,19]. To build a robust, compact and cost-effective fluorescence-suppressed Raman devices, sensors utilizing time-gated single-photon avalanche diodes (SPADs) fabricated in standard high-voltage complementary metal-oxide-semiconductor (HVCMOS) process have been introduced to the field [20,21]. The high fluorescence rejection capability of time-gated CMOS SPAD-based Raman spectrometers have been already demonstrated in the analysis of fluorescent pharmaceuticals [22,23].

The further development of the SPAD line sensors has led to more practical and compact time-resolved CMOS SPAD Raman sensors utilizing the basic concept of time-correlated single-photon counting (TCSPC) procedure [19–21]. The CMOS technology enables the integration of all TCSPC electronics, such as delay units, time-to-digital converters (TDCs) and histograms, to the same application-specific integrated circuit with the SPAD line sensor itself, significantly reducing the overall complexity of the equipment compared to the more traditional TCSPC Raman devices based on either a SPAD or some other detector solution. A great advantage of time-resolved measurement over the conventional constant-size time-gating approach is that the width of the time gate, which is used to separate the Raman signal from the fluorescence tail, can be modified even in the data post-processing phase in order to obtain the best possible Raman signal-to-noise ratios.

In this work, a Raman spectrometer based on a previously developed time-resolved CMOS SPAD line sensor [19] was utilized in the label-free investigations of Metronidazole and Vitamin C diffusivities as a function of ANFC hydrogel concentrations. The results are interesting for the modulation of ANFC-based implants and drug delivery systems, when the release rate needs to be set to a desired value. But more importantly, the method is universal and can be adapted to any hydrogel/drug combination for producing reliable drug diffusion coefficient data in complex and heterogeneous systems, where traditional sampling-based methods are cumbersome to use. The wide temporal range of the

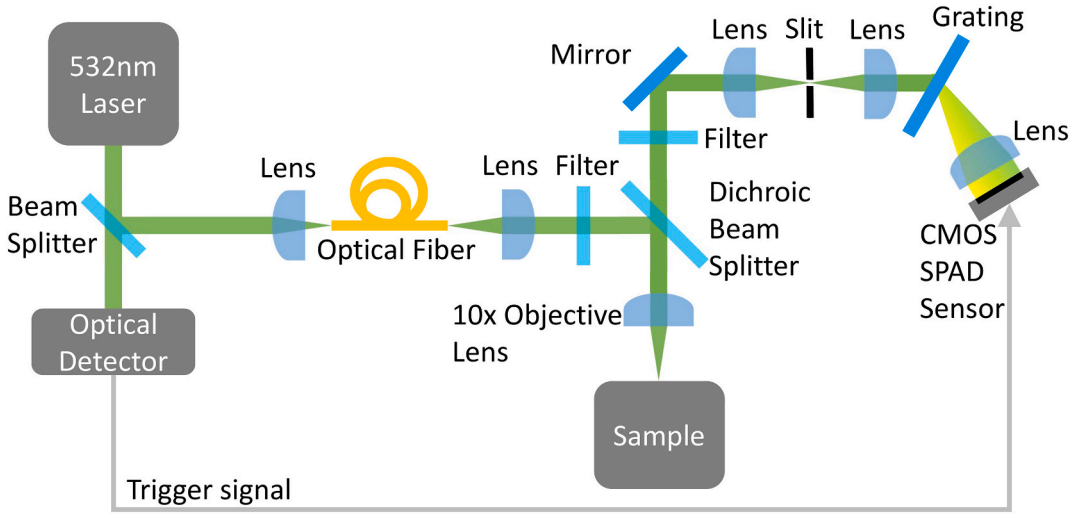

Fig. 2. Block diagram of the time-resolved Raman and fluorescence spectrometer.

employed time-resolved CMOS SPAD sensor makes it possible to capture also the fluorescence decay of samples, giving rise to a combined time-resolved Raman and fluorescence spectroscopy, which provides additional information on the chemical, functional and structural changes in samples [24].

2. Materials and methods

The drug molecules Metronidazole and Vitamin C (Fig. 1) as dry powder were purchased from Merck (Sigma Aldrich, St Louis, USA) and 0.9% ANFC hydrogel was purchased from UPM (GrowDex®-T, UPM Biomedicals, Helsinki, Finland). 0.9% ANFC hydrogel concentrations used were 0.9%, 0.45% and 0.225% diluted with the Milli-Q water.

The time-resolved Raman spectrometer was an in-house built custom spectrometer, whose block diagram is shown in Fig. 2. It was built mainly using off-the-shelf optomechanical and optical elements from three major component vendors (Thorlabs, Edmund Optics and Newport) and was designed to operate at 180-degree excitation and collection geometry. A 532 nm wavelength pulsed laser (TEEM photonics, France, model: ANG-500P-CHS) is used as an excitation source. The pulse width and repetition rate of the laser are 150 ps full width at half maximum (FWHM) and 300 kHz, respectively and the average optical power used was 208 mW. Most of the optical power is delivered to a sample through a microscope objective but a small fraction (~2%) is guided to the trigger detector to synchronize the time-resolving CMOS SPAD line sensor for measuring the time-of-arrival of backscattered photons from the sample.

The time-resolved CMOS SPAD sensor was fabricated in 0.35 μm HVCMOS technology and consists of an 8 × 256 SPAD array and a 256-channel on-chip TDC with the temporal resolution of 20 ps. The temporal range of the TDC was set here to 82 ns. The pitch of SPADs within the spectral axis is 41.6 um defining a wavenumber resolution of ~7 cm^{-1} and a wavenumber range of ~1800 cm^{-1} for the whole Raman spectrometer. The data read-out procedure of the sensor currently limits the maximum frame rate of the system to 100 kframes/s and thus, the repetition rate of the laser cannot be fully utilized.

The high temporal resolution and the wide temporal range of the sensor with simultaneous recording on all spectral points makes it possible to record 3-D data of collected photons from the sample (intensity vs. time vs. wavenumber). Therefore, Raman and fluorescence photons can be separated in time-domain and ns-scale fluorescence lifetimes can be estimated by post-processing the recorded 3-D data. The post-processing of the data is done by using custom-made MATLAB scripts (MathWorks, USA) and includes, for example, the formation of the normal 2D (intensity vs wavenumber) Raman spectra with the desired time gate widths as well as the dark count and baseline correction and filtering of the formed spectra. A detailed description of the used time-resolved CMOS SPAD line sensor is given in reference [13].

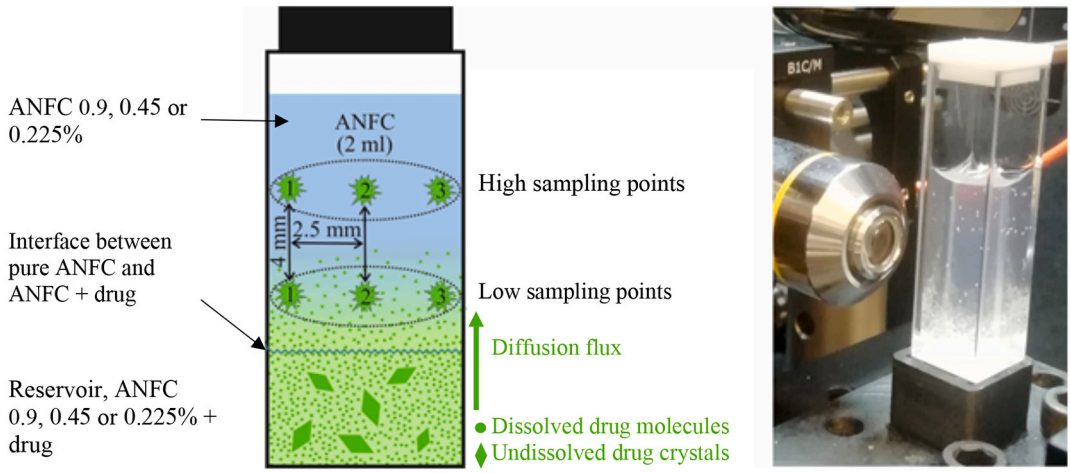

Fig. 3. Schematic picture and photograph of the sample configuration, the reservoir and the pure ANFC had the same hydrogel concentration.

Drug diffusion and mass transfer measurements. The reservoir, containing the ANFC and drug with the drug concentrations exceeding the aqueous drug solubility by ca. 5 times, was prepared at least 24 h prior the experiment, mixed vigorously and stored at +4C allowing the partial dissolution of the drug particle into the ANFC. 0.75 ml of ANFC containing the drug was pipetted to the bottom of a 3.5 ml fused quartz cuvette (Thorlabs, USA, model: CV10Q3500F) and layered on top with 2 ml of the pure ANFC having the same cellulose concentration as that of the reservoir (Fig. 3). The amount of the drug is high enough to assume that the reservoir maintains roughly the same drug concentration throughout and during the measurements since the total volume of ANFC (2.75 ml) is not enough to completely dissolve the drug. The prepared sample was then placed to a sample holder coupled with an XYZ translation state with standard micrometers (Thorlabs, USA, model: PT3/M) to enable accurate laser focusing. In total, two horizontal and three vertical laser focus locations, i.e. sampling points, were used in this study, as shown in Fig. 3. The lower sampling points were ~ 2.5 mm above the surface between the drug/ANFC dispersion and pure ANFC and the higher sampling points were 4 mm above the lower sampling points.

The time-resolved Raman and fluorescence spectra from the different sampling points were always obtained in the same order (from the first acquisition point to the last): lower 1, lower 2, lower 3, higher 3, higher 2 and higher 1 (numbering refers to Fig. 3). The Metronidazole samples were studied for 48 h and the Vitamin C ones for 120 h. Because the used spectrometer setup currently requires manually controlled data acquisition, the measurements were conducted only during the daytime, accordingly; – day 1, 0–10 h; day 2, 23–30 h; day 3,46.5–48 h. The release was further monitored with Vitamin C samples by applying three additional sampling times at 72 h, 96 h and 120 h. The sampling interval during the days was 30 min and the spectra were recorded by shooting 10 million laser pulses to the sample, resulting in an acquisition time of 100 s per sampling point with the spectrum frame rate of ~100 kframes/s.

The Raman signal used in the diffusion coefficient calculations was derived from the time-gated Raman spectra obtained with 600 ps collection window achieved by summing up 30 adjacent time bins in the data post-processing phase. That enables the collection of all the Raman scattered photons generated by the laser pulses while at the same time rejecting major part of the fluorescence and other background radiation from ambient light. All the measurements were conducted in an open environment with regular laboratory lighting condition at room temperature and atmosphere. Room temperature was maintained constant at 22 °C. The fluorescence lifetime was determined from the fluorescence decay curves at wavenumber areas where no Raman scattered signals and peaks were detected.

The fluorescence lifetime analysis was only done with Vitamin C because Metronidazole does not have significant fluorescence. The fluorescence decay curves were formed by sweeping a 100 ps wide photon collection window through the time axis with steps of 20 ps (done in the data pots-processing phase) in order to achieve additional signal averaging. Furthermore, the fluorescence intensity was defined as the summed intensity of wavenumber range of 1852–2022 cm^{-1}, which presents the pure fluorescence without Raman. The fluorescence lifetimes were estimated with the free DecayFit software [25], which uses iterative re-convolution with a least-squares analysis. The bi-exponential decay function, $A_1 \cdot e^{\left(-t/\tau_1\right)} + (1-A_1)\cdot e^{\left(-t/\tau_2\right)}$, was fitted to the obtained decay curves, since this offered better fitting results than the single-exponential model.

3. Theoretical section

Fick's second law in one dimension (Eqs. 1 and 2) was used to fit the data obtained by Raman scattering and fluorescence:

$$\frac{\partial f}{\partial t} = D\frac{\partial^2 f}{\partial x^2} \tag{1}$$

$$\frac{\partial f}{\partial x} = 0, x = H = 2\ \text{cm}, t > 0; f = 1, x = 0\ \text{cm}, t > 0; f = 0, t = 0, x > 0; \tag{2}$$

where D is the diffusion coefficient (cm^2/s), f is the normalized concentration of the drug, t is the time (s), x the distance from the drug/ANFC dispersion and initially empty ANFC solution, and H is the height of the empty ANFC phase. The concentrations are replaced here with f to represent the fraction of the drug concentration of the total aqueous solubility of the drug, i.e. a normalized concentrations ($f = c/c_S$). The geometry in this case is non-standard as the diffusion is confined to a fixed length. As boundary conditions, c at the lower interface is kept constant at the solubility of the drug (c_S) by the presence of dissolving drug powder, and the drug gradient at the top ($x = H$) is zero.

Eq. (1) can be solved as a sum of complementary error functions:

$$f = \sum_{n=0}^{\infty}\left((-1)^n erfc\frac{2nH + x}{2\sqrt{Dt}} + (-1)^n erfc\frac{(2n+2)H - x}{2\sqrt{Dt}}\right) \tag{3}$$

As the exact solution given by Eq. (3) is somewhat complex, an approximation of the diffusion coefficient can be obtained by first considering the case of semi-infinite diffusion, where the diffusion would not be confined to a fixed length H. The solution to Eq. (1) in this case can be readily obtained as

$$f = erfc\frac{x}{2\sqrt{Dt}} \tag{4}$$

Eq. (4) can be expanded as Taylor's series to yield even simpler approximation if $\frac{x}{2\sqrt{Dt}}$ is further assumed to be smaller than one:

$$erfc\frac{x}{2\sqrt{Dt}} \approx 1 - \frac{x}{\sqrt{\pi Dt}} \tag{5}$$

It is good to remember that this equation only applies when there is no meaningful saturation occurring in the initially empty ANFC phase. It therefore applies to a limited period where a clear diffusion front has been established ($2\sqrt{Dt} > x$) but the concentration at the top is still quite close to zero. Regardless, this simplified solution can be useful for a quick estimation of diffusion coefficients, since with two horizontal sampling locations as are used here, eqs. (4) and (5) can be used to get

$$\Delta f = \frac{\Delta h}{\sqrt{\pi Dt}} \tag{6}$$

$$\mathrm{D} = \frac{1}{\pi t}\left(\frac{\Delta h}{\Delta f}\right)^2 \tag{7}$$

where Δf is the difference in the normalized concentrations and Δh the height separation between the high and low sampling points.

In practice, the estimated diffusion coefficients based on Eq. (7) need to be further adjusted by using the exact solution of Eq. (3) to account for possible non-linearities such as saturation during the experiments. However, there was a practical problem in using the correct solution, since when working with viscous hydrogels, it is very hard to fix the initial lower interface at an exact height. This means that even though Δh can be fixed, the exact values of x for the two measurement points are unknown. Fortunately, when two measurement heights are used, we have the additional benefit that the real locations can be estimated by calculating the ratio of $1 - f$ values at these two locations (high and low):

$$\frac{1 - f_{high}}{1 - f_{low}} = \frac{x_{high}}{x_{low}} = \alpha$$

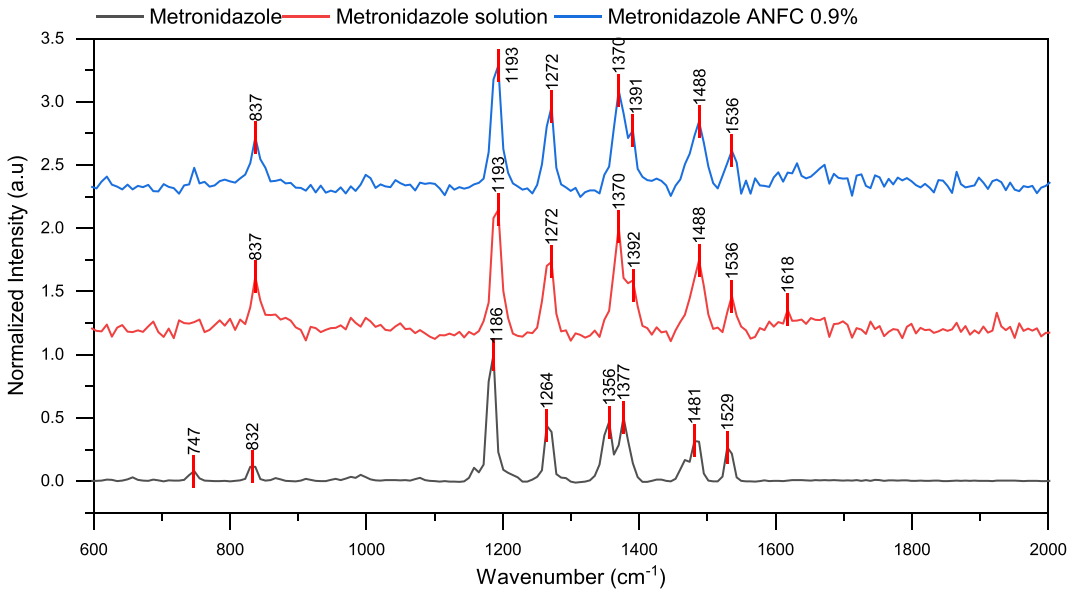

Fig. 4. The Raman spectra of Metronidazole in solid form (black), in water (red), and in 0.9% ANFC hydrogel-water solution (blue). (For interpretation of the references to colour in this figure legend, the reader is referred to the web version of this article.)

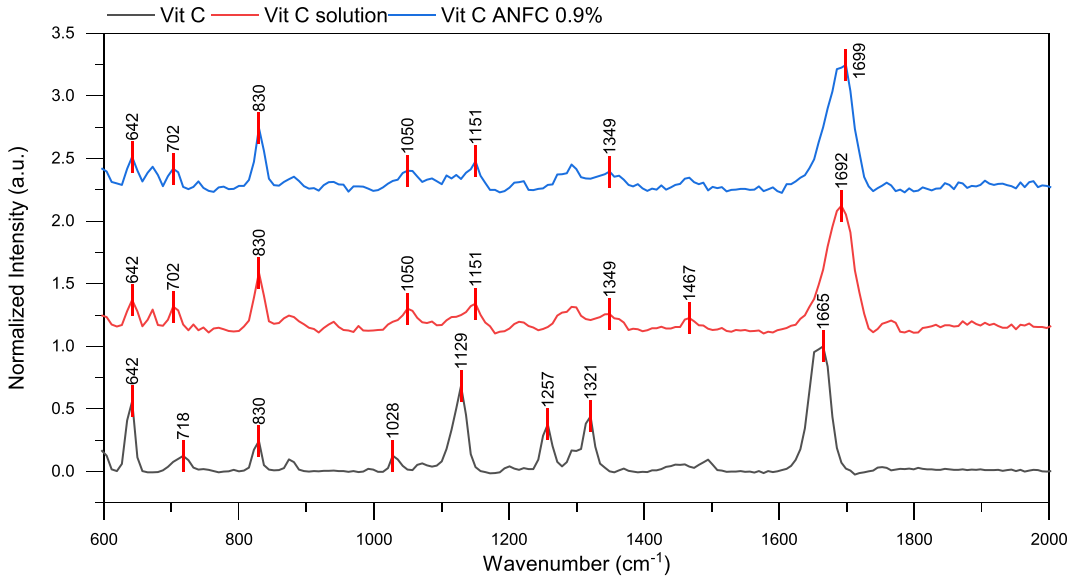

Fig. 5. The Raman spectra of Vitamin C in solid form (black) in water (red) and in 0.9% ANFC hydrogel-water solution (blue). (For interpretation of the references to colour in this figure legend, the reader is referred to the web *version of this article.)*

$$x_{low} = \frac{\Delta h}{\alpha - 1}$$

The final workflow for determining the diffusion coefficients in ANFC hydrogels can be found in Supporting Information together with the normalization of the data obtained.

4. Results

Before starting the analysis for diffusion constants of the studied drugs, the Raman spectra of ANFC in water, and Metronidazole and Vitamin C in solid form, in water and in 0.9% ANFC hydrogel-water were measured (Figs. 4 and 5).

The vibrations assigned for Metronidazole and Vitamin C are shown in Tables 1 and 2. Raman peak amplitudes were used to estimate drug concentration used in the equations shown in the Theoretical section. In order to obtain the normalized concentrations (f), the Raman peak amplitudes at the different time points were divided by the ones of the saturated aqueous solution of the concerned drug. The used Raman peak amplitudes were the most relevant ones for taking into account the molecular structure for Metronidazole were at 1193 cm^{-1}, 1264 cm^{-1}, 1370 cm^{-1} and 1488 cm^{-1}, and the ones for Vitamin C were at 830 $cm^{-1}$and 1692 cm^{-1}.

One of the novelties of the present study is that the diffusion constants can be calculated based on the Raman peak intensities, and the fluorescence decay time that was measured simultaneously, as shown in Fig. 6 (Vitamin C samples), can give extra information about e.g. drug-cellulose interactions.

As can be seen based on the Tables 1 and 2 wavenumber and intensity of the Raman peaks, some molecular level interactions may

Table 1
Assignment of Metronidazole vibrations as Raman shifts (cm^{-1}).

Metronidazole in solid state	Metronidazole in water	Metronidazole in ANFC	Assignment
746 (w)			CH_2 rock
837 (w)	837 (w)	832(w)	Ring breathing
865 (vw)			CH_3 rock, sigma CH_2
910 (vw)			Gamma CH_2, CH_2 rocking
951 (vw)			sigma OH
1077 (vw)			CH
1160 (sh)			C-C, CH
1186 (s)	1193 (s)	**1193 (s)**	**v C-N**
1264 (m)	1272 (m)	**1272 (m)**	**N-O**
1356(m)	1370 (s)	**1370 (s)**	**v C—N aromatic**
1377 (m)	1392(sh)	1392(sh)	CH_2 scissor, sigma CH3
1481 (m)	1488 (m)	**1488 (m)**	**C=O, sigma asymmetric CH_3**
1529 (m)	1536 (w)	1536 (w)	C=C

vw = very weak; w = weak, m = medium, s = strong.

Table 2
Assignment of vitamin C vibrations as Raman shifts (cm^{-1}).

Vitamin C in solid state	Vitamin C in water	Vitamin in ANFC	Assignment
642 (s)	642 (vw)	642 (vw)	OH out-of-plane deformation C—C ring stretching
718 (w)	702 (vw)	702 (vw)	OH out-of-plane deformation
830 (s)	830 (s)	**830 (m)**	**C-C ring stretching**
1028 (w)	1050 (w)	1050 (w)	C-O-H bending, C-O-C stretching
1129 (s)	1151 (vw)	1151 (vw)	C-O-C stretching
1257 (m)	–	–	C-O-H bending (twisting)
1321 (m)	1349 (vW)	1349 (vw)	CH bending (wagging)
1453 (vw)	1467 (vw)	1467 (8vw)	CH bending
1665 (s)	1692 (s)	**1692 (s)**	**C=C ring stretching**

vw = very weak; w = weak, m = medium, s = strong.

occur, but these seem to be very minor, as is the change in fluorescence decays in various ANFC samples (see Fig. 6). This indicates that direct chemical binding of the drug moieties to ANFC is weak and the expected changes in the diffusion coefficients are most likely dependent on the physical characteristics of ANFC, i.e. restriction of diffusion pathways due to the porosity and tortuosity of the cellulose network. Furthermore, the Raman spectra peaks were constant over time for both their position and relative intensities (Fig. 7), indicating that no drug degradation was taking place during the experiment.

The diffusion constants of the drugs were calculated as explained above. The diffusion data measured with Raman along with the fitted values according to Eq. (3) are shown in Fig. 8 for Vitamin C and Fig. 9 for Metronidazole. Table 3 lists the fitted diffusion coefficients. In the case of Metronidazole, the saturation of the top ANFC phase caused strong nonlinear effects on the concentration profiles and the exact solution was needed for proper estimation of D. In the case of Vitamin C, the diffusion would have been possible to model also with the simpler Eq. (4), and estimate D with Eq. (7). It seems that there is no strong effect of ANFC concentration for the diffusivity of Vitamin C in this concentration range, which is quite logical for a small hydrophilic drug. Moreover there seems to be no differences between the diffusion of Vit C in ANFC and water, this observation have been reported in other studies where is suggested that ANFC hydrogels affect the drug diffusion at concentration higher than 3% [26]. There seems to be a stronger correlation between the diffusion coefficient and ANFC concentration in the case of metronidazole. Metronidazole seems to defuse faster in lower concentration of ANFC then in higher concentrated ANFC or water which would indicate that the important characteristic for mass transport in nanofibrillar cellulose would be the hydrophobicity of the drug [27]. The lack of a strong correlation between hydrogel concertation and diffusion speed might be due to the heterogeneous pore size of the ANFC, which display a pore size distribution between ~1 to 100 μm [28], however, more thorough understanding of the underlying factors, a large screening study might be needed.

5. Discussions

Based on the presented results above, we were able to show, that it is possible to follow the drug diffusion and mass transfer in an unstirred hydrogel environment by on-line, label-free, fluorescence- and background-suppressed Raman spectra, and simultaneously obtain the information of the fluorescence decay times. Drug diffusivities were evaluated for the first time in unstirred hydrogels on-line by following the amplitude of the Raman peaks of the studied drugs, while simultaneously evaluated drug fluorescence decays were used to verify possible binding or drug degradation was taking place. It is not the first time that a spectroscopic technique is used for diffusivity studies [10,32], however in the previous study, UV–vis spectroscopy was chosen. The phenomena behind UV spectroscopy are the absorption and emission of the UV light which has a wavelength (λ) from 200 nm to 700 nm. The absorption and the emission depend on chemical nature of the analyte. Therefore, the energy difference between the electronically excited absorption and emission is dissipated into the radiation less intersystem crossing from the electronically excited states to the first electronically excited state and its lowest vibrational state. That radiation less

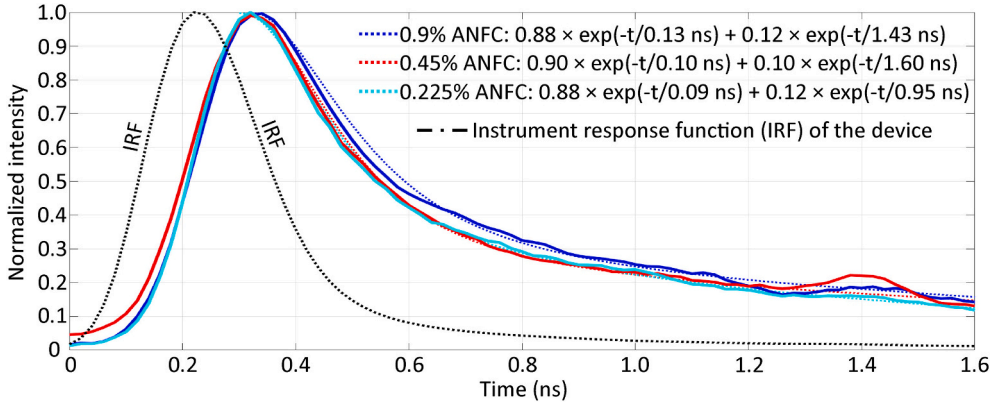

Fig. 6. Fluorescence decay curves with the different ANFC concentrations formed by taking the average of the time points 24 h, 48 h and 120 h (solid lines). Dotted lines present the bi-exponential fitting curves, whose equations are shown in the top-right corner.

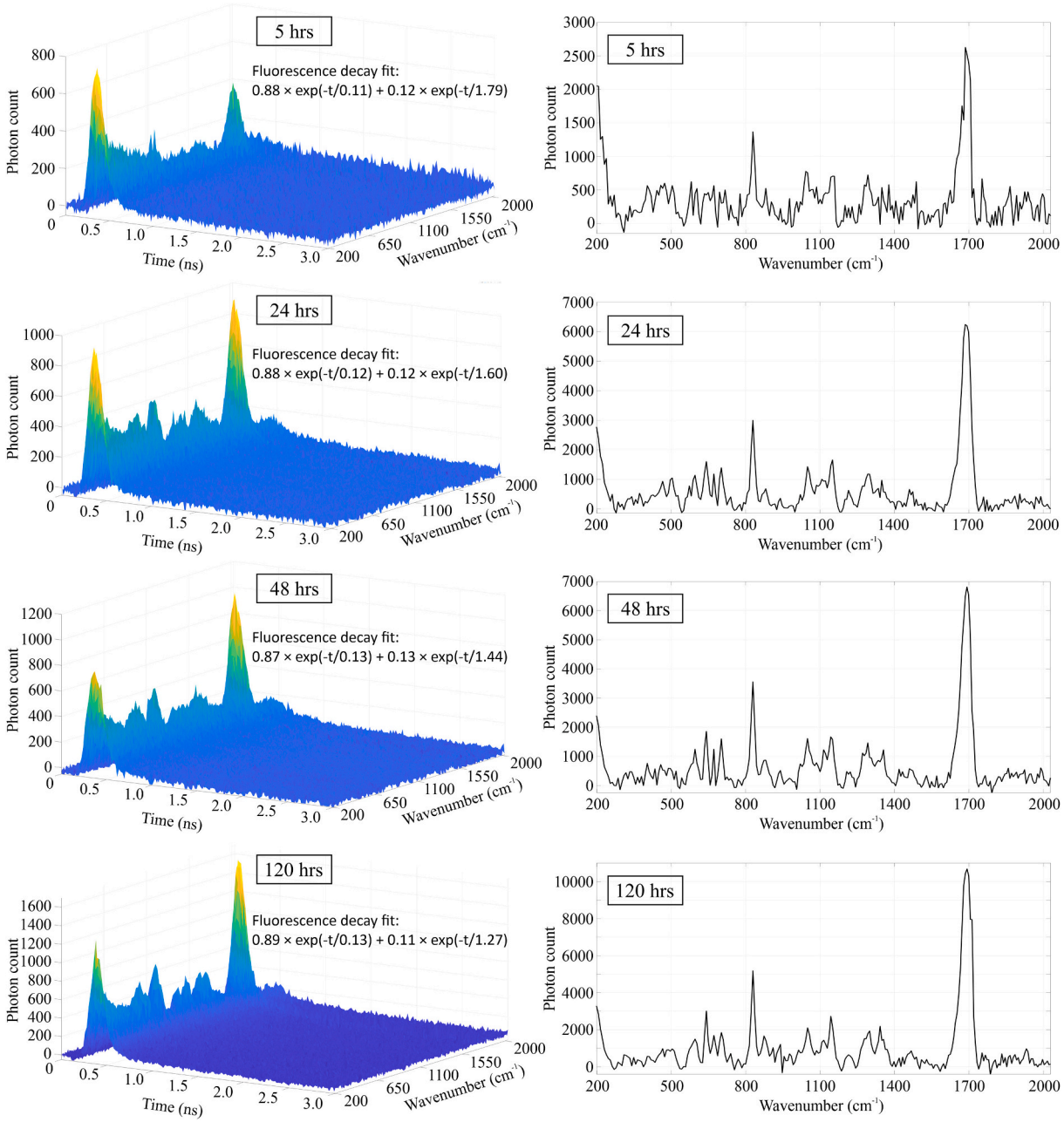

Fig. 7. The combined 3D time-resolved Raman and fluorescence spectra of Vitamin C measured after 5 h, 24 h, 48 h and 120 h in 0.9% anionic nanofibrillated cellulose (ANFC) hydrogel (left side figures). Right side figures show the post-processed time-gated Raman spectra with the time gate width of 600 ps. The data was collected from the lower sampling point 2.

intersystem crossing may heat the sample, and therefore may also affect its diffusion coefficient. Moreover, in UV–vis spectroscopy the absorption intensity to calculate the diffusion is at the most cases detected only in one wavelength, thus it cannot provide exhaustive information on the drug nor its environment. The Raman spectroscopy is based on the inelastic scattering of light, which is an event that occurs at the lower energy compared to the UV–vis absorption. Raman spectra are able to reveal the chemical nature of the samples, as well its physical status, while the fluorescence lifetime changes in its environment. However, in our case, the effect of the ANFC hydrogel concentration on the fluorescence decay was practically negligible.

Raman technology has progressed strongly during the last twenty years for applications in the biomedical field. Crucially, it offers a solution to one of the biggest problems in drug analytics, intrinsic drug fluorescence, which can be avoided by using the time-gated Raman technology. That has now also been shown in the case of the Raman analysis of the EVs [22] and could be applied in the future for other Raman analysis of biomolecules. Equally importantly, it is unaffected by the presence of water and is not measured in transmission mode. This uniquely makes it suitable for drug analytics in heterogeneous hydrogels, which intrinsically have high water contents and efficiently scatter incoming light. The possibility to simultaneously detect the fluorescence intensity and decay times reveals yet another important parameter to monitor concerning the drug release. The decay times are sensitive to changes in the environment of the drugs, while the intensity makes it possible to directly monitor the release of fluorescent drugs and biomolecules. All these measurements were shown to be possible to perform on-line and label-free.

Raman spectroscopy is known to be sensitive to molecular level changes [23]. Therefore, the developed system can also be utilized to

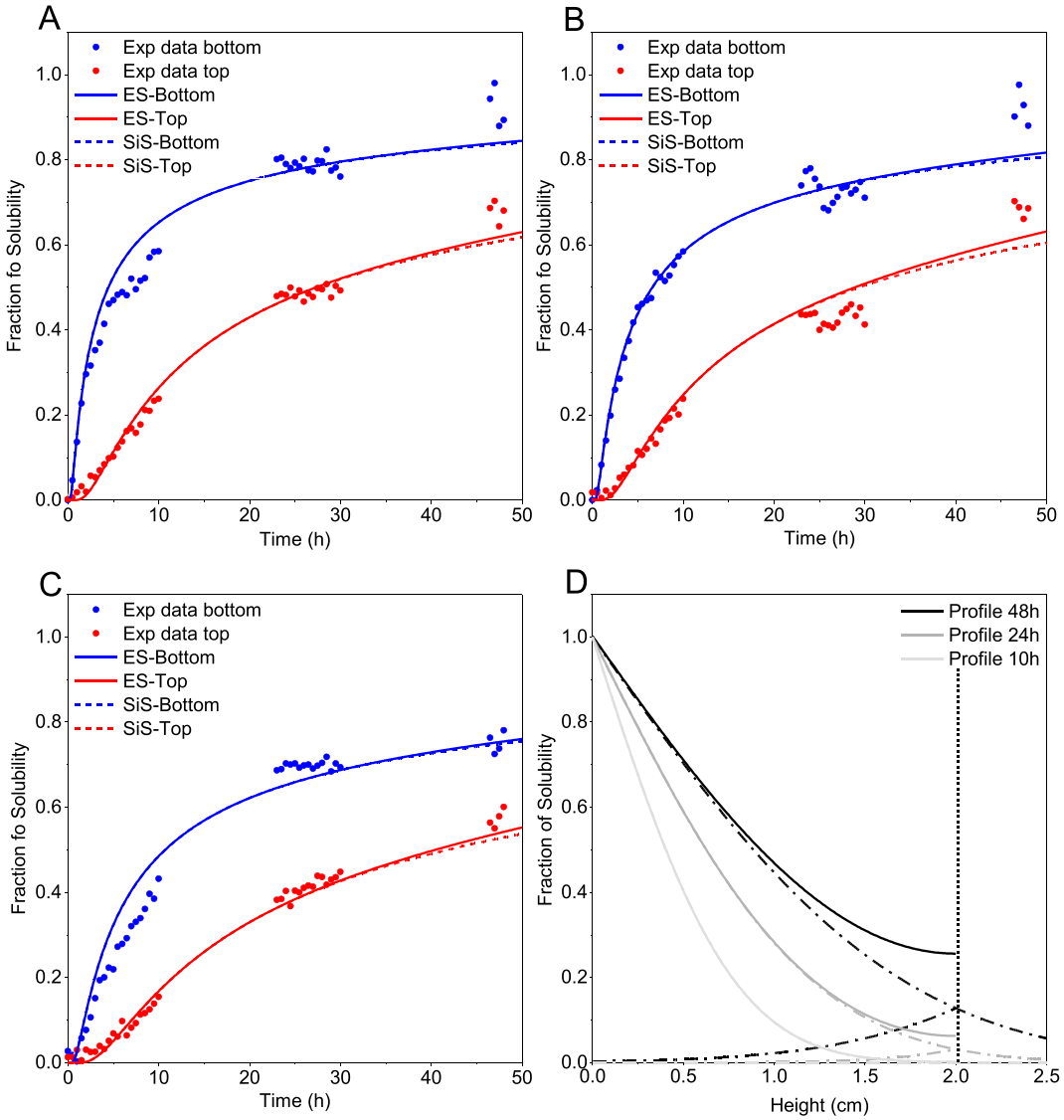

Fig. 8. A, B, C: Vitamin C normalized concentrations in ANFC vs. time. The ANFC concentration was either 0.9% (A), 0.45% (B), or 0.225% (C). Symbols show measured values based on Raman measurements and lines show theoretical values obtained by the from Eq. (3). Blue symbols/lines are from the lower measurement position, while red symbols/lines are from the higher measurement position. **D:** Simulated concentration vs. height profile at different time points for measurements done in 0.225% ANFC. The dashed line shows what the results of a semi-infinite solution would look like. The "reflected" curve shows the difference to the exact solution. (For interpretation of the references to colour in this figure legend, the reader is referred to the web version of this article.)

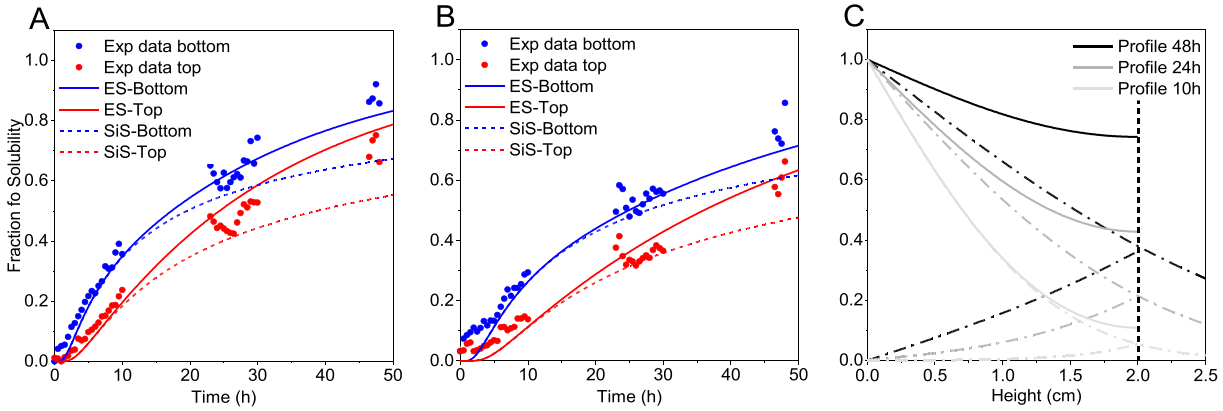

Fig. 9. A, B: Metronidazole normalized concentrations in ANFC vs. time. The ANF concentration was either 0.225% (A) or 0.45% (B). Symbols show measured values based on Raman measurements and lines show theoretical values from eq. Blue symbols/lines are from the lower measurement position, while red symbols/lines are from the higher measurement position. **C:** Simulated concentration vs. height profile at different time points for measurements done in 0.225% ANFC. The dashed line shows what the results of a semi-infinite solution would look like. The "reflected" curve shows the difference to the exact solution. (For interpretation of the references to colour in this figure legend, the reader is referred to the web version of this article.)

Table 3
Diffusion coefficients of Vitamin C and Metronidazole in various ANFC concentrations based on Raman measurements and theoretical fitting, and the values fin water found at the literature.

	D in 0.225% ANFC ($x10^{-6}$ cm^2/s)	***D*** in 0.45% ANFC ($x10^{-6}$ cm^2/s)	***D*** in 0.9% ANFC ($x10^{-6}$ cm^2/s)	D in water ($x10^{-6}$ cm^2/s)
Vitamin c	5.0	6.0	4.8	5.32 ± 0.26[29] 6.8 ± 0.6[30]
Metronidazole	15	10	N.d.	4.3[31]

follow the drug stability during drug release studies and the long-term stability of the drugs in hydrogels. The method could be further extended to the study of e.g. the diffusion of biomedical proteins in hydrogels, and detect their short- and long-term stabilities and denaturation rates, which cannot be otherwise easily evaluated on-line. This would also be of great value for the automatization of the manufacturing process of controlled release systems and implants, for example. Based on the findings, it would be then easy to adjust the formulation parameters such as thickness, drug loading, or cellulose content and modulate the drug release rate to be relevant in terms of the pharmacokinetics of the drug.

6. Conclusion

Our study shows that detailed and comprehensive information about drug diffusion kinetics in ANFC can be obtained with a simple experimental set-up. Our study also highlights the power of the combined real time label-free time-resolved Raman and fluorescence/fluorescence lifetime analysis for drug release analytics to be applied into the field of bio- and pharmaceuticals enabling the real time label-free analysis of the payloads also in pharmaceutical hydrogels for further applications in the field.

Author statement

Conceptualization MY, IN, JZ, JK; Methodology JZ, JK; Software TL, JZ, JK, TT, PK; Validation All; Investigation MY, IN, JZ, JK; Resources MY, IN, AM; Writing Original draft MY, IN, JZ, JK, VK; Writing-Review editing All; Supervision MY, IN, AM; Funding acquisition MY, IN, AM.

Acknowledgements

This work was supported by the Academy of Finland grants n:o 314406 (MY), n:o 314404 (IN), n:o 323719 (IN), n:o 314405 (AM).

Appendix A. Supplementary data

Supplementary data to this article can be found online at https://doi.org/10.1016/j.jconrel.2021.04.032.

References

[1] J.L. Drury, D.J. Mooney, Hydrogels for tissue engineering: scaffold design variables and applications, Biomaterials 24 (2003) 4337–4351.
[2] Y. Cheng, X. Luo, G.F. Payne, G.W. Rubloff, Biofabrication: programmable assembly of polysaccharide hydrogels in microfluidics as biocompatible scaffolds, J. Mater. Chem. 22 (2012) 7659–7666.
[3] D. Klemm, et al., Nanocelluloses: a new family of nature-based materials, Angew. Chem. Int. Ed. 50 (2011) 5438–5466.
[4] M. Pääkkö, et al., Enzymatic hydrolysis combined with mechanical shearing and high-pressure homogenization for nanoscale cellulose fibrils and strong gels, Biomacromolecules 8 (2007) 1934–1941.
[5] J. Vartiainen, et al., Health and environmental safety aspects of friction grinding and spray drying of microfibrillated cellulose, Cellulose 18 (2011) 775–786.
[6] T. Saito, S. Kimura, Y. Nishiyama, A. Isogai, Cellulose nanofibers prepared by TEMPO-mediated oxidation of native cellulose, Biomacromolecules 8 (2007) 2485–2491.
[7] T. Hakkarainen, et al., Nanofibrillar cellulose wound dressing in skin graft donor site treatment, J. Control. Release 244 (2016) 292–301.
[8] R. Koivuniemi, et al., Clinical study of nanofibrillar cellulose hydrogel dressing for skin graft donor site treatment, Adv.Wound Care 9 (2019) 199–210.
[9] A.C.F. Ribeiro, M.A. Esteso, Transport properties for pharmaceutical controlled-release systems: a brief review of the importance of their study in biological systems, Biomolecules 8 (2018) 178.
[10] M.P. di Cagno, et al., Experimental determination of drug diffusion coefficients in unstirred aqueous environments by temporally resolved concentration measurements, Mol. Pharm. 15 (2018) 1488–1494.
[11] E. Smith, G. Dent, Modern Raman Spectroscopy: A Practical Approach, Wiley, 2019.
[12] A. Paudel, D. Raijada, J. Rantanen, Raman spectroscopy in pharmaceutical product design, Adv. Drug Deliv. Rev. 89 (2015) 3–20.
[13] F.G. Vogt, M. Strohmeier, Confocal UV and resonance Raman microscopic imaging of pharmaceutical products, Mol. Pharm. 10 (2013) 4216–4228.
[14] S. Wartewig, R.H.H. Neubert, Pharmaceutical applications of mid-IR and Raman spectroscopy, Adv. Drug Deliv. Rev. 57 (2005) 1144–1170.
[15] D. Shendi, et al., Hyaluronic acid as a macromolecular crowding agent for production of cell-derived matrices, Acta Biomater. 100 (2019) 292–305.
[16] T. Vankeirsbilck, et al., Applications of Raman spectroscopy in pharmaceutical analysis, TrAC Trends Anal. Chem. 21 (2002) 869–877.
[17] R.P. Van Duyne, D.L. Jeanmaire, D.F. Shriver, Mode-locked laser Raman spectroscopy. New technique for the rejection of interfering background luminescence signals, Anal. Chem. 46 (1974) 213–222.
[18] D.V. Martyshkin, R.C. Ahuja, A. Kudriavtsev, S.B. Mirov, Effective suppression of fluorescence light in Raman measurements using ultrafast time gated charge coupled device camera, Rev. Sci. Instrum. 75 (2004) 630–635.
[19] P. Matousek, et al., Fluorescence suppression in resonance Raman spectroscopy using a high-performance picosecond Kerr gate, J. Raman Spectrosc. 32 (2001) 983–988.
[20] I. Nissinen, A. Länsman, J. Nissinen, J. Holma, J. Kostamovaara, 2×(4×)128 time-gated CMOS single photon avalanche diode line detector with 100 ps resolution for Raman spectroscopy, in: 2013 Proceedings of the ESSCIRC (ESSCIRC), 2013, pp. 291–294, https://doi.org/10.1109/ESSCIRC.2013.6649130.
[21] J. Kostamovaara, et al., Fluorescence suppression in Raman spectroscopy using a time-gated CMOS SPAD, *Opt. Express,* OE 21 (2013) 31632–31645.
[22] T. Rojalin, et al., Fluorescence-suppressed time-resolved Raman spectroscopy of pharmaceuticals using complementary metal-oxide semiconductor (CMOS) single-photon avalanche diode (SPAD) detector, Anal. Bioanal. Chem. 408 (2016) 761–774.
[23] T. Lipiäinen, et al., Time-gated Raman spectroscopy for quantitative determination of solid-state forms of fluorescent pharmaceuticals, Anal. Chem. 90 (2018) 4832–4839.
[24] K. Suhling, P.M.W. French, D. Phillips, Time-resolved fluorescence microscopy, Photochem. Photobiol. Sci. 4 (2005) 13–22.
[25] DecayFit, Fluorescence Decay Analysis - The fluorescence laboratory. http://www.fluortools.com/software/decayfit.
[26] H. Paukkonen, et al., Nanofibrillar cellulose hydrogels and reconstructed hydrogels as matrices for controlled drug release, Int. J. Pharm. 532 (2017) 269–280.
[27] H. Aisala, et al., Linking volatile and non-volatile compounds to sensory profiles and consumer liking of wild edible Nordic mushrooms, Food Chem. 304 (2020) 125403.
[28] J.J. Sheard, et al., Optically transparent anionic nanofibrillar cellulose is cytocompatible with human adipose tissue-derived stem cells and allows simple imaging in 3D, Stem Cells Int. 2019 (e3106929) (2019).
[29] Greg Gerhardt, R.N. Adams, Determination of diffusion coefficients by flow injection analysis, Anal. Chem. 54 (1982) 2618–2620.
[30] G. Zou, Z. Liu, C. Wang, Flow injection analysis methods for determination of diffusion coefficients, Anal. Chim. Acta 350 (1997) 359–363.
[31] A. Meulemans, F. Paycha, P. Hannoun, M. Vulpillat, Measurement and clinical and pharmacokinetic implications of diffusion coefficients of antibiotics in tissues, Antimicrob. Agents Chemother. 33 (1989) 1286–1290.
[32] F. Ye, et al., Real-time UV imaging of drug diffusion and release from Pluronic F127 hydrogels, Eur. J. Pharm. Sci. 43 (2011) 236–243.